Reduction of Radiation Efficiency in High-Speed Jets

Dimitri Papamoschou,[*] Juntao Xiong [†] and Feng Liu [‡]

University of California, Irvine, Irvine, CA, 92697, USA

The Lighthill acoustic analogy indicates that substantial noise reduction is possible in high-speed jets by reducing the radiation efficiency. This entails reducing the convective Mach number of the eddies whose footprint is sensed in the near pressure field. In dual-stream jets, local reduction in convective Mach number is possible by inducing asymmetry in the plume that redistributes the most energetic eddies from the fast inner stream to the slower outer stream on the underside of the jet. Assuming that the convective velocity of the most energetic eddies is the mean velocity at the location of the peak turbulent kinetic energy, a RANS-based acoustic analogy predicts with reasonable fidelity the noise reduction measured experimentally. Importantly, it is shown that the reduction in the source strength is caused primarily by the reduction in radiation efficiency. A large eddy simulation of a single-stream high-subsonic jet allows determination of the convective velocity through space-time correlations throughout the computational domain. The convective velocity at the edge of the jet, defined as the boundary between the inner rotational field and the outer linear pressure field, is close to the mean axial velocity at the location of peak kinetic energy. This provides a tool for RANS-based acoustic analogy models to accurately predict the radiation efficiency and its reduction.

Nomenclature

a	=	speed of sound
A	=	cross sectional area; amplitude
C	=	correlation coefficient
H	=	wavenumber-frequency spectrum
k	=	turbulent kinetic energy
L	=	characteristic length scale
M	=	Mach number
M_c	=	convective Mach number
r	=	distance between source and observer
R	=	observer distance in spherical coordinate system; correlation function
$\widehat{R}$	=	Fourier transform of correlation function
p	=	static pressure
T	=	Lighthill stress tensor
u, v, w	=	velocities in Cartesian coordinate system
u_*	=	characteristic velocity scale
U	=	fully-expanded velocity
U_c	=	convective velocity
x, Y, z	=	Cartesian coordinate system
y	=	radial coordinate
U_c	=	convective velocity
α	=	acoustic wavenumber $= \omega/a_\infty$
$\boldsymbol{\alpha}$	=	wavenumber vector in direction of observer $= \alpha\mathbf{x}/R$
β	=	shape parameter

[*]Professor, Department of Mechanical and Aerospace Engineering, Fellow AIAA
[†]Postdoctoral Researcher, Department of Mechanical and Aerospace Engineering, Member AIAA
[‡]Professor, Department of Mechanical and Aerospace Engineering, Fellow AIAA

American Institute of Aeronautics and Astronautics

γ	=	specific heat ratio
Γ	=	azimuthal influence function
ϵ	=	dissipation
θ	=	polar angle relative to jet axis
ϕ	=	azimuthal angle relative to downward vertical
ρ	=	density
ω	=	angular frequency
Ω	=	specific dissipation $= \epsilon/k$

Subscripts

p	=	primary (core) exhaust
s	=	secondary (bypass) exhaust
∞	=	ambient (flight) conditions

I.   Introduction

Noise from the exhaust of jet engines continues to be an environmental and health problem. The challenge is particularly severe for low-bypass, high-performance turbofan engines used on tactical aircraft and envisioned for next-generation supersonic transports. Today, research on high-speed jet noise is primarily motivated by the need for tactical supersonic aircraft to become more environmentally acceptable. A related aspect is the exposure of carrier-deck personnel to extremely high sound pressure levels, which can cause hearing loss and other adverse health effects.[1] Solutions for tactical aircraft are bound to benefit future supersonic business jets that have similar operational characteristics.

Noise reduction concepts for high-speed jets have taken numerous forms and have generated a large body of literature. A comprehensive review can be found in a recent paper by Morris and McLaughlin.[2] Despite the scale of this effort, a cohesive framework for noise reduction has not been well developed. The Lighthill acoustic analogy provides valuable guidance for establishing such a framework. In its most general form, to be reviewed in Section II, it suggests three fundamental means for suppressing the noise source: (a) reduction in turbulence intensity; (b) reduction in coherence length scales; and (c) reduction in radiation efficiency. We will argue that the last method, reduction in radiation efficiency, offers the most potent means for achieving noise suppression in high-speed jets. The paper will elaborate on the modeling of jet noise, with emphasis on predicting radiation efficiency, using the Reynolds Averaged Navier Stokes (RANS) computed flow field. Large Eddy Simulation (LES) of a high-subsonic jet provides support for the key assumptions in the RANS-based model.

The radiation efficiency (the ability of turbulent motion to generate sound that propagates to the far field) peaks when the motion of turbulent eddies in the jet is supersonic relative to the surrounding medium. The effect is manifested as Mach wave radiation from eddies traveling with a convective Mach number $M_c > 1$, as illustrated by the left image of Fig. 1. The direction of propagation of the Mach waves (complementary to the Mach angle) is given by $\cos\theta = 1/M_c$, or $M_c \cos\theta - 1 = 0$. This expression will be seen again in the formulation of the acoustic analogy model. Surrounding the supersonic jet with a slower secondary flow can significantly weaken the Mach wave radiation,[3] as shown on the right image of Fig. 1. This approach has been the basis of noise reduction efforts in coaxial and offset dual-stream nozzles,[3–8] and can be explained physically as a consequence of the motion of eddies in the primary jet becoming subsonic relative to the secondary flow. However, it is more insightful to view the changes in the acoustic field as a result of the reduced radiation efficiency of the flow in the bottom image. Introduction of the secondary stream reduced the radiation efficiency of the jet, an effect captured vividly by the images of Fig. 1. We put this concept in a more general framework using the Lighthill acoustic analogy as a guide.

II.   Acoustic Analogy Model

We cover only the salient aspects of the theory, with details available in a variety of publications including Refs. 9 and 10. Referring to Fig. 2, the noise source region has volume $\mathcal{V}$, location $\mathbf{y}$ refers to a point inside the source region, location $\mathbf{x}$ is the observer location outside the source region, $r = |\mathbf{x} - \mathbf{y}|$ is the distance
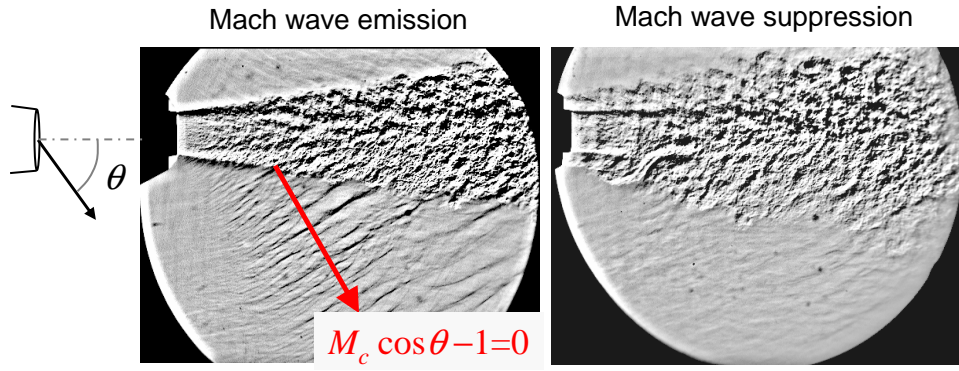
Mach wave emission   Mach wave suppression

$M_c \cos\theta - 1 = 0$

Figure 1. Schlieren images of Mach wave radiation and its suppression in a jet with velocity of 700 m/s (Ref.2).
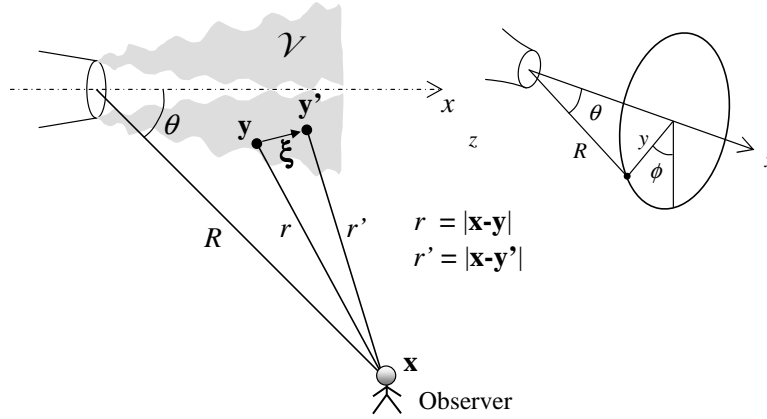

Figure 2. Nomenclature and coordinate system for acoustic analogy model.

between source and observer, and $\boldsymbol{\xi} = \mathbf{y}' - \mathbf{y}$ denotes the separation vector between two source elements. In the far field, $r \approx R$ and the wavenumber vector $\boldsymbol{\alpha} = \alpha\mathbf{x}/R$ describes the propagation of sound towards the observer. The spectral density of pressure in the far field takes the form

$$S(\mathbf{x}, \omega) = \alpha^4 \int_{\mathcal{V}} |G(\mathbf{x}, \mathbf{y}, \omega)|^2 \, H(\mathbf{y}, \boldsymbol{\alpha}, \omega) \, d^3\mathbf{y} \tag{1}$$

with

$$H(\mathbf{y}, \boldsymbol{\alpha}, \omega) = \int_{\mathcal{V}_\xi} \int_{-\infty}^{\infty} R_{xxxx}(\mathbf{y}, \boldsymbol{\xi}, \tau) \exp\left[i(\boldsymbol{\alpha} \cdot \boldsymbol{\xi} - \omega\tau)\right] d\tau \, d^3\boldsymbol{\xi} \tag{2}$$

Here $G(\mathbf{x}, \mathbf{y}, \omega)$ is a Greens function that describes the propagation of the sound from the source to the observer; $H(\mathbf{y}, \boldsymbol{\alpha}, \omega)$ is the wavenumber frequency spectrum of the equivalent noise sources in the acoustic analogy; and R_{xxxx} is the space-time correlation of the Lighthill stress tensor in the direction of the observer. Equation 2 is a four-dimensional Fourier transform of the space-time correlation over time and over the correlation volume $\mathcal{V}_\xi$. A general form for the space-time correlation is

$$R_{xxxx}(\mathbf{y}, \boldsymbol{\xi}, \tau) = A_{xxxx}(\mathbf{y}) \, R_1\left(\frac{\xi_x}{L_\tau(\mathbf{y})}\right) R_2\left(\frac{\xi_y}{L_y(\mathbf{y})}\right) R_3\left(\frac{\xi_\phi}{L_\phi(\mathbf{y})}\right) R_4\left(\frac{\xi_x - \widetilde{u}\tau}{L_x(\mathbf{y})}\right) \tag{3}$$

$A_{xxxx}(\mathbf{y})$ is the amplitude of the correlation and has units of $\rho^2 u^4$; $R_1 \ldots R_4$ are correlation functions; L_x, L_y, and L_ϕ are correlations length scales in the axial, radial and circumferential (azimuthal) directions, respectively; L_τ is a length scale that depends on the turbulent time scale τ_*; and $\widetilde{u}$ is a characteristic velocity associated with the convection of the mean flow or the convection of the turbulent eddies. Expecting the contribution of "shear noise" to dominate the direction of peak emission, we set $A_{xxxx} = B \, \overline{\rho}^2 \, \overline{u}^2 k$, where

B is a fitting constant. Assuming that the correlations do not have azimuthal variation, the four-dimensional Fourier transform of Eq. 2 yields:

$$H(\mathbf{y}, \boldsymbol{\alpha}, \omega) \ = B \ \overline{\rho}^2 \ \overline{u}^2 k \ L_\tau L_y L_\phi \frac{L_x}{\widetilde{u}} \ \widehat{R}_1 \left(\alpha L_\tau \frac{\widetilde{u} \cos\theta - a_\infty}{\widetilde{u}} \right) \ \widehat{R}_2 \left(\alpha L_y \sin\theta \right) \ \widehat{R}_3(0) \ \widehat{R}_4 \left(\frac{\omega L_x}{\widetilde{u}} \right) \qquad (4)$$

We may select $\widetilde{u}$ to be the mean flow velocity or the convection velocity of the turbulent eddies. The two velocities can be very different. In this study we set $\widetilde{u} = U_c$ where U_c is the convection velocity of the large-scale structures, consistent with the focus of our work on modeling noise in the direction of peak emission. Then the convective Mach number $M_c = \widetilde{u}/a_\infty = U_c/a_\infty$ represents the Mach number of large-scale structures (instability waves) with respect to the ambient medium. On selecting $L_\tau = U_c \tau_*$, Eq. 4 becomes

$$H(\mathbf{y}, \boldsymbol{\alpha}, \omega) \ = B \ \overline{\rho}^2 \overline{u}^2 k \ \tau_* L_x L_y L_\phi \ \widehat{R}_1 \left(\omega \tau_* (M_c \cos\theta - 1) \right) \ \widehat{R}_2 \left(\alpha L_y \sin\theta \right) \ \widehat{R}_3(0) \ \widehat{R}_4 \left(\frac{\alpha L_x}{M_c} \right) \qquad (5)$$

The radiation efficiency term $\widehat{R}_1$ contains the $M_c \cos\theta - 1$ factor discussed in Section I. Equation 5 suggests three fundamental ways to reduce noise within a fairly constant source volume $\mathcal{V}$ in Eq. 1:

1. *Reduction in turbulence intensity (amplitude term).* This necessitates large reduction in turbulent kinetic energy k to achieve significant noise suppression. Even if k were reduced by 50%, the maximum noise reduction would be around 3 dB.

2. *Reduction of the coherence time and length scales .* While breakup of the large eddies is possible near the nozzle, the extent to which structures at large distances from the nozzle can be affected is not clear, given the natural tendency of the shear layer self-organize into large vortical motions.

3. *Reduction of the radiation efficiency.* To illustrate the potency of this approach, consider a reduction in M_c from 1.2 to 0.8. For Strouhal number Sr near unity, the magnitude of the $\omega \tau_*$ term in the argument is ~ 30, based on RANS simulations to be presented later. Assuming an exponential form for the correlation $R_1(x) = \exp(-|x|)$, its Fourier transform is $\widehat{R}_1(\eta) = 2/(1 + \eta^2)$. Figure 3 illustrates the impact of the M_c reduction on the radiation efficiency term. For M_c=1.2, $\eta = 0$ in the direction $\theta = 35°$, indicating peak radiation efficiency (Mach wave emission). Reducing M_c to 0.8 results in a roughly 50-fold decline of the radiation efficiency term. This is consistent with spectral decline of 10-15 dB measured at $Sr \sim 1$ for jets where M_c was similarly reduced.
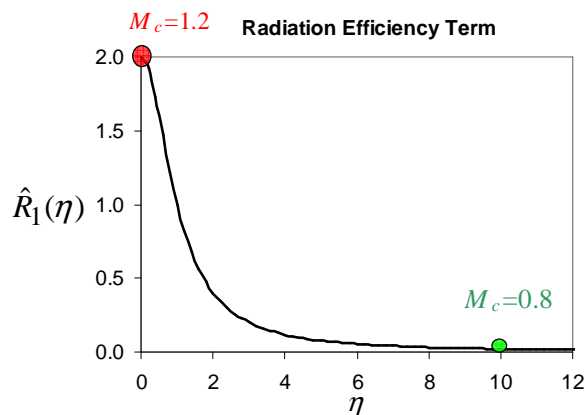

Figure 3. Radiation efficiency term of Eq. 5 for Strouhal number one and for the flow discussed in Section III.

In recent work[9] the acoustic analogy model was parameterized in terms of the shapes of the correlation functions and the coefficients of the correlation scales. The generic correlation function was selected as

$$R_j(t) \ = \ e^{-|t|^{\beta_j}} \qquad (6)$$

American Institute of Aeronautics and Astronautics

The correlation length and time scales followed the usual constructions based on the turbulent kinetic energy k and specific dissipation $\Omega = k/\epsilon$ of the RANS-computed flow:

$$
\begin{aligned}
L_x &= C_1 \frac{k^{1/2}}{\Omega} \\
L_y &= C_2 \frac{k^{1/2}}{\Omega} \\
L_\phi &= C_3 \frac{k^{1/2}}{\Omega} \\
\tau_* &= C_4 \frac{1}{\Omega}
\end{aligned}
\tag{7}
$$

Assuming equality of radial and circumferential correlations (i.e., $\beta_3 = \beta_2$, $C_3 = C_2$) the far-field spectral density becomes a function of the parameter vector $[C_1, C_2, C_4, \beta_1, \beta_2, \beta_4]$. The parameter vector was determined by matching, in a least-squares sense, the experimental spectral density for a baseline jet in a particular polar direction. In the computations that follow, the baseline jet was a coaxial jet that produced an axisymmetric mean flow field. The exact same parameter vector determined for the baseline jet was applied to jets issuing at the same thermodynamic exit conditions but with asymmetric distortion of the plume.

For the baseline (axisymmetric) jet, the Green's function G in Eq. 1 takes the free-field form

$$
G = \frac{1}{4\pi R} e^{-i\alpha R}
\tag{8}
$$

For asymmetric jets, the Green's function needs to account for propagation through the mean flow, a task that formally requires solution of the linear Euler equations. However, considerable simplification is possible by neglecting propagation through the mean flow and applying outward linear propagation from the very-near acoustic field using wavepacket models. The neglect of propagation through the mean flow is supported by a simple 2D sound transmission model as well as experimental evidence of weak azimuthal coherence of the acoustic near field.[11] The weak coherence suggests a very large transmission loss of sound through the jet. The wavepacket model describes how a localized azimuthal disturbance spreads with radial distance and polar angle. These effects are integrated into a Green's function of the form

$$
G = \frac{1}{4\pi R} e^{-i\alpha R} \, \Gamma\left(\phi(\mathbf{x}) - \phi(\mathbf{y}), \theta(\mathbf{x}), \alpha\right)
\tag{9}
$$

where $\phi(\mathbf{y})$ is the azimuthal angle of a given source volume element; and $\theta(\mathbf{x})$ and $\phi(\mathbf{x})$ are the polar and azimuthal coordinates of the far-field observer, respectively.

The selection of a coordinate system for defining the azimuthal angle ϕ is critical. The nozzle axis is a poor choice as the fan flow deflectors impart a downward tilt to the jet plume and deform the cross-sectional shape. In previous work we used the centroid of the momentum flux to define the "center" of the jet at a given axial location,[9]

$$
Y_c(x) = \frac{\int_{A(x)} \overline{\rho}\,\overline{u}^2 Y\, dA}{\int_{A(x)} \overline{\rho}\,\overline{u}^2\, dA}
\tag{10}
$$

where Y is the transverse coordinate on the symmetry plane and $A(x)$ is the cross-sectional area of the plume at a given axial location x. Once the centroid is computed, the $Y-$coordinates of all the data are reset to a new frame (by subtracting $Y_c(x)$) where $Y = 0$ is the centroid location.

III.   Review of Jet Flows

This section describes the experimental and computational data for the jets to which the acoustic analogy methodology is applied. The jets have been the subject of previous publications,[12] so this section summarizes only the information pertinent to the present study. Aeroacoustic tests were conducted in U.C. Irvine's Jet Aeroacoustics Facility, a subscale facility that uses helium-air mixtures for replicating the exhaust velocity and density of hot jets. Jet noise was recorded by a moveable far-field microphone array consisting of eight 3.2-mm condenser microphones (Bruel & Kjaer, Model 4138). The experiment utilized a separate-flow coaxial

American Institute of Aeronautics and Astronautics

plug nozzle designed for bypass ratio BPR=2.7. The fan exit diameter was $D_s = 28.1$ mm and the fan exit height was 1.8 mm. The acoustic tests were performed with the primary flow at fully-expanded velocity $U_p = 600$ m/s and fully-expanded Mach number $M_p = 1.03$. The corresponding values for the secondary flow were $U_s = 400$ m/s and $M_s = 1.15$. These conditions were enabled using cold helium-air mixture jets, which have been shown to match very well the acoustics of hot air jets. The Reynolds number of the jet, based on fan diameter, was 0.92×10^6.

Fan flow deflection was achieved through the use of internal airfoil-shaped vanes that spanned the width of the annulus of the fan nozzle. A large number of vane configurations were tested. For this paper, we examine only one of the cases, labeled "4Va." It comprised two pairs of vanes, one pair mounted at azimuthal angle $\phi = 90°$ and the other at $\phi = 150°$. The vane cross section was a NACA 7564 airfoil with chord length of 3.0 mm. The vane trailing edge was located 2.0 mm upstream of the fan exit plane.

The computational fluid dynamics code used here is known as PARCAE[12] and solves the unsteady three-dimensional Navier-Stokes equations on structured multiblock grids using a cell-centered finite-volume method. Information exchange for flow computation on multiblock grids using multiple CPUs is implemented through the MPI (Message Passing Interface) protocol. In its time-averaged implementation, the code solves the RANS equations using the JST scheme[13] and the Shear Stress Transport (SST) turbulence model of Menter.[14] The SST model combines the advantages of the k-Ω and k-ϵ turbulence models for both wall-bounded and free-stream flows. In its unsteady implementation, the solver uses implicit backward three-layer second-order time integration with explicit five stage Runge-Kutta dual time stepping. The time-evolving jet flow is simulated using a hybrid RANS/LES approach. The spatial discretization of the inviscid flux is based on the weighted averaged flux-difference splitting algorithm of Roe.[15, 16] The viscous flux is discretized using a second-order central difference scheme. The time-evolving jet flow is simulated using a hybrid RANS/LES approach.[17, 18] Near the wall region the Spalart-Allmaras turbulence model[19] is used to model the turbulent viscosity, while in the free shear flow the computation relies on the subtle dissipation of the upwind scheme, using the method proposed by Shur *et al.*[16]

For the RANS simulation of dual-stream jets, the computational grid extended $3.8D_s$ radially from the nozzle centerline and over $20D_s$ downstream of the nozzle. The base nozzle grid had 3.7 million grid points and the 4Va grid had 5.8 million grid points. Figure 4 plots contour maps of the mean axial velocity $\overline{u}$ and turbulent kinetic energy k on the symmetry plane. The deflection causes thickening of the flow in the downward direction and significant reduction of the turbulence intensity on the underside of the jet. The region of zero or near-zero k in the vicinity of the axis of the nozzle is a good indication of the extent of the potential core. Note that the centroid, as defined in Eq. 10, passes exactly through the point where this region ends.
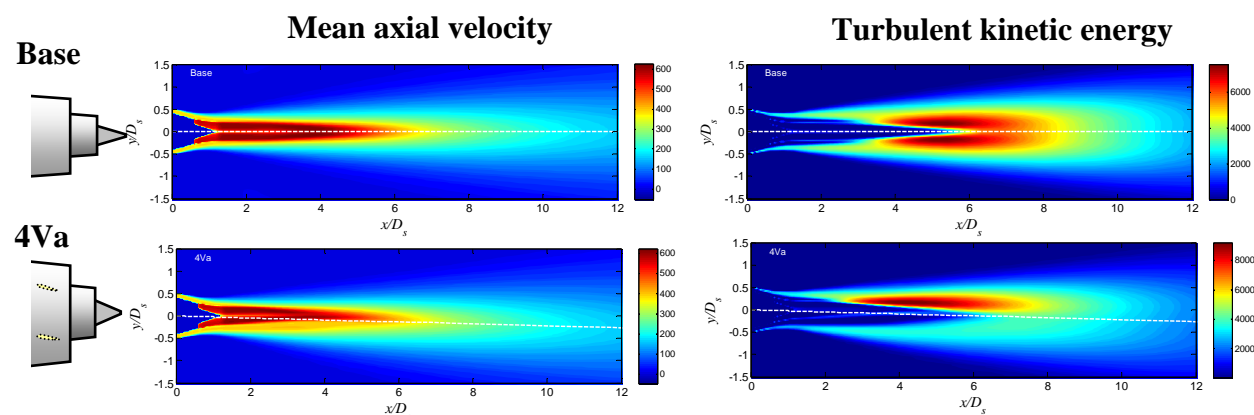

Figure 4. RANS predictions of mean axial velocity (m/s) and turbulent kinetic energy (m^2/s^2) fields for the Base and 4Va jets. Dashed line indicates centroid location.

IV. Selection of Convective Velocity and Resulting Far-Field Spectral Density

As is evident in the $\widehat{R}_1$ term of the wavenumber-frequency spectrum (Eq. 5), the convective Mach number plays a vital role on the radiation efficiency, particularly when M_c is high subsonic or supersonic.

When $M_c \cos\theta = 1$ a volume element radiates with 100% efficiency in the direction θ. Detailed hot-wire measurements of space-time correlations in a subsonic jet[20] indicate that the convective speed U_c varies with radial location, following the mean velocity $\overline{u}$ but with a smaller radial gradient than $\overline{u}$. It was thus suggested that setting $U_c = \overline{u}$ is a reasonable approximation. However, when dealing with large-scale "coherent" structures, that is, structures that span the integral length scale of the shear layer, the appropriateness of using $U_c = \overline{u}$ should be questioned, particularly in high-speed jets. First, eddies with $U_c = \overline{u}$ cannot emit Mach waves (they are intrinsically subsonic), which is contrary to the vast experimental evidence of Mach wave emission. Second, there is strong experimental evidence, starting from the seminal works of Brown and Roshko,[21] that coherent structures have one convective velocity over their lifetime.[22, 23]

Because our work tries to model noise in the direction of peak emission, the choice $M_c = \overline{u}/a_\infty$ appears problematic for the reasons delineated above. In the absence of a time-resolved solution that would yield the space-time correlations directly (a laborious task experimentally or computationally), we seek guidance from the RANS simulation. We associate the convective velocity with the motion of the most energetic eddies, which presumably would be at the locus of the peak turbulent kinetic energy. The locus of peak k is a surface around the jet axis defined by the radial location $y_m(x,\phi)$ where k is maximized at given axial location x and azimuthal angle ϕ. Letting $\mathbf{y} = (x, y, \phi)$ represent the location of a volume element in polar coordinates (Fig. 2), the convective Mach number of this volume element is defined as

$$M_c(x, y, \phi) \;=\; \frac{\overline{u}(x, y_m(x,\phi), \phi)}{a_\infty} \tag{11}$$

This means that all the volume elements at a particular x and ϕ are assigned the same value of M_c corresponding to the local maximum of k. A similar definition for M_c was used by Karabasov $et\ al.$[24] where the convection velocity was determined from the location of the maximum in the fourth-order velocity cross-correlation. Next we evaluate the impact of this assumption on the modeling of the far-field spectral densities for the baseline and deflected jets.
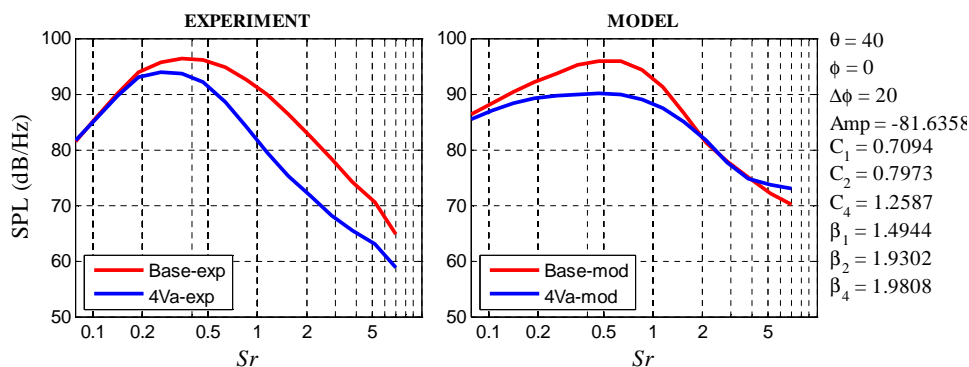

Figure 5. Experimental and modeled spectra for jet 4Va (blue curves) with comparison to the Base jet (red curves). Model uses the traditional definition of convective Mach number. Optimized parameter vector is displayed on the right.

IV.A. Results for $M_c = \overline{u}/a_\infty$.

Using the "traditional" definition of convective Mach number $M_c = \overline{u}/a_\infty$, the distribution of M_c is proportional to that of the mean velocity profile shown in Fig. 4. The result of the parameterization is shown in Fig. 5, which displays the modeled and experimental spectra at $\theta = 40°$ for cases Base and 4Va, along with the optimized parameter vector (which, as discussed previously, is obtained by least-squares matching of the experimental and modeled spectra of the Base case). The model produces a fair, but not very good, match of the Base spectrum. The prediction of the spectrum for jet 4Va is poor. Noise reduction is predicted for low frequency, but there is no noise reduction above $Sr \sim 1$. Despite the significant reduction in turbulent kinetic energy on the underside of the jet, the model fails to predict the downward noise reduction measured experimentally.

American Institute of Aeronautics and Astronautics

IV.B. Results for $M_c = \overline{u}(x, y_m(x, \phi))/a_\infty$.

Now we implement the more physical definition of convective velocity as the mean axial velocity at the location of peak turbulent kinetic energy. It is instructive to view that location on cross-sectional contours of the turbulent kinetic energy. Figure 6 plots the k contours for cases Base and 4Va on the symmetry plane; the dashed lines indicate the locus of peak k on the bottom ($\phi = 0°$) and top ($\phi = 180°$) sides of the jet. For the Base jet, the location of peak k is initially in the outer shear layer then shifts inward to the inner shear layer once the outer potential core is dissipated. For the 4Va jet, the location of peak k on the top side follows the same trend as in the Base jet; however, on the bottom side the locus remains in the outer shear layer well past the end of the primary potential core. The corresponding axial distributions of M_c are plotted in Fig. 7. For the Base jet, M_c starts at low value of 0.6, jumps to supersonic value of 1.18 at $x/D_s = 3$, then gradually decays with downstream distance. The initially low value is because the dominant source is the outer shear layer between the secondary stream ($U_s = 400$ m/s) and the ambient. Once the secondary core is dissipated at $x/D_s \approx 4$ the inner shear layer ($U_p = 600$ m/s) is exposed to the ambient and becomes the dominant noise source, resulting in the jump of M_c. The initial value of M_c corresponds to U_c/U_s=0.52 and the peak value corresponds to U_c/U_p=0.68. Both ratios are in line with prevailing models for the convective speed in compressible shear layers.[22] For jet 4Va we note a sharp reduction of the convective Mach number in the downward direction, with its peak value declining from 1.18 for the Base jet to 0.82 for jet 4Va. This is because the locus of peak k on the bottom side of the jet shifts to the low-speed region of the outer shear layer.

The predictions of the far-field spectral densities are plotted in Fig. 8. There is a very good match of the baseline spectrum, and a reasonable prediction of the noise reduction of jet 4Va. Spectral reductions at $Sr = 1$ are near 10 dB. It is important to realize that the prediction of noise reduction is predicated on a proper definition of convective Mach number, which underscores the role of the radiation efficiency discussed earlier. Note that the axial correlation function has $\beta_1 = 1.18$, i.e., it is close to the exponential decay assumed in Section II.
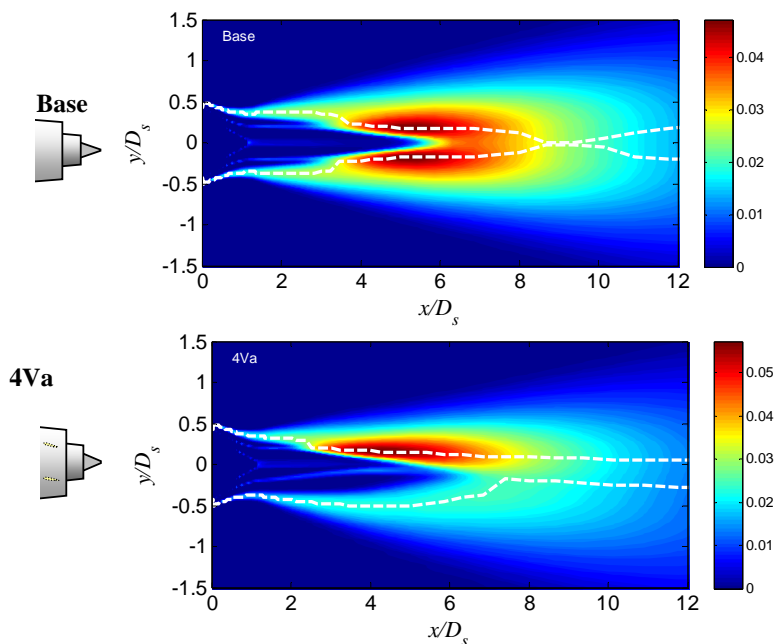

Figure 6. Turbulent kinetic energy contours on symmetry plane, including locations of peak value (dashed lines).

IV.C. Source Components

It is instructive to assess the distribution of the source and its main components in Eq. 5, in order to evaluate their relative impacts on the noise reduction predicted in Fig. 8. We examine the wavenumber-frequency spectrum H and its following components: the turbulent kinetic energy, k; the radiation efficiency term $L_x \widehat{R}_1$; and the correlation volume $L_x L_y L_z$. Figure 9 presents these distributions at $Sr = 1.16$ as contour

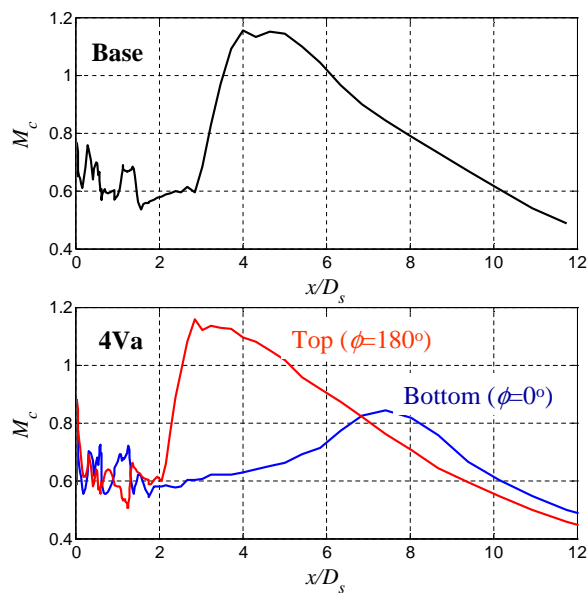American Institute of Aeronautics and Astronautics

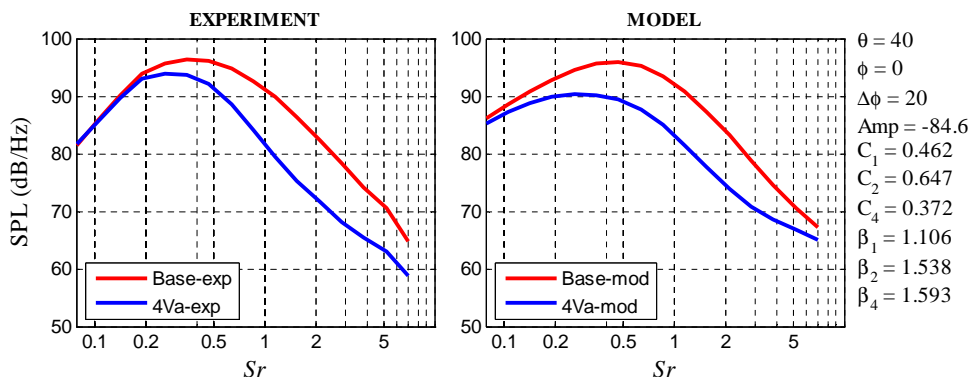**Figure 7. Axial distribution of convective Mach number.**

Figure 8. Experimental and modeled spectra for jet 4Va (blue curves) with comparison to the Base jet (red curves). Model uses a convective Mach number based on the velocity of the most energetic eddies. Optimized parameter vector is displayed on the right.

plots of the local maximum (in the radial direction) on the $x - \phi$ plane. The contour values are in decibels to facilitate connection to the spectral data of Fig. 8. For this Strouhal number, the total source per unit volume H peaks near $x/D_s = 4$. At that location, we note a decline of about 20 dB in the downward direction ($\phi = 0°$). The reduction in turbulent kinetic energy can account for at most 2 dB of that decline. The correlation volume exhibits insignificant changes. On the other hand, the radiation efficiency is reduced dramatically, by about 15 dB, as anticipated by the preliminary arguments in Section II. Looking at the similarity between the contours of H and $L_x \widehat{R}_1$ it is evident that the distribution of H is dominated by the radiation efficiency term. This explains the failure of the "traditional" M_c formulation to predict the spectral decline, and underscores once again the potency of noise suppression via reduction of the radiation efficiency.

V.   LES Computations

The preceding has brought up an important question. Given a RANS-predicted jet flow field, what is a proper selection for the convective velocity that provides an accurate quantification of the radiation efficiency term in Eq. 5? The RANS computation gives only two independent pieces of statistical information: the turbulent kinetic energy k and the dissipation. We showed that selecting the convective velocity to be
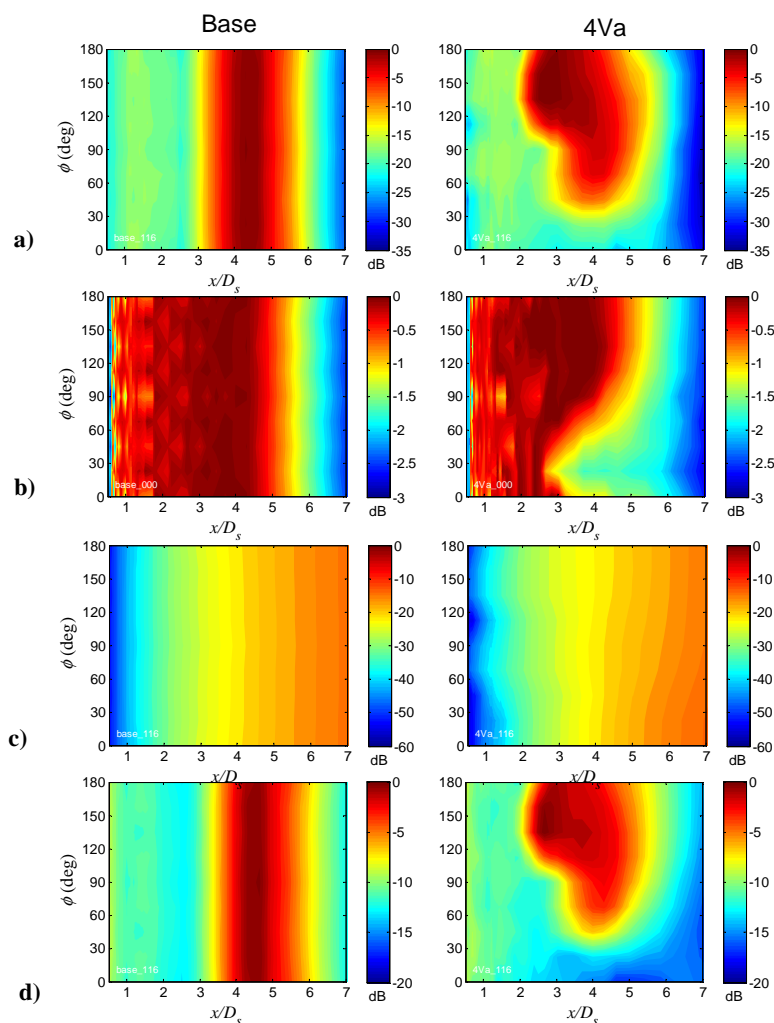
American Institute of Aeronautics and Astronautics

Figure 9. Distributions of source and its components at $Sr = 1.16$**. Local maximum (along radial direction) is plotted versus axial distance** x **and azimuthal angle** ϕ**. a) Wavenumber frequency spectrum** H**; b) turbulent kinetic energy** k**; c) correlation volume** $L_x L_y L_z$**; and d) radiation efficiency term** $L_x \widehat{R}_1$**.**

the velocity at the location of peak k produced physically meaningful distributions for the convective Mach number and, importantly, allowed a reasonable prediction of the noise reduction in asymmetric jets. However, our hypothesis needs further physical justification. The advent of time-resolved computations of the jet flow field, using large eddy simulation (LES), allows us to evaluate the rigor of our assumption. Because LES is very expensive computationally, it cannot replace the RANS-based acoustic analogy as a practical noise prediction tool. However, LES provides a wealth of information that can inform the RANS/AA model towards physically meaningful modelling of the key ingredients of acoustic analogy, namely the space-time correlations.

V.A. LES of Mach 0.9 Jet

Because of resource limitations, LES was applied to a single-stream jet with exit diameter $D_j = 0.0218$ m. The jet was supplied by room-temperature air and exhausted at $M_j = 0.9$ and $U_j = 286$ m/s. The acoustic Mach number is U_j/a_∞=0.83 and the Reynolds number is 300,000 based on exit diameter. The same jet was tested in our aeroacoustics facility where the far-field spectra were measured.

The PARCAE code reviewed in Section III was used to compute the unsteady flow. The computational grid extended to about $20D_j$ in the radial direction and $60D_j$ in the axial direction. The grid had about 7 million grid points. For the nozzle flow, the total pressure, total temperature, and zero flow angle were specified at the inlet surface corresponding to a perfectly expanded exit Mach number. For the ambient

American Institute of Aeronautics and Astronautics

region surrounding the nozzle flow, a non-reflecting characteristic boundary condition was imposed, and a buffer layer was implemented near the outflow. The adiabatic no-slip boundary condition was specified on the nozzle wall.
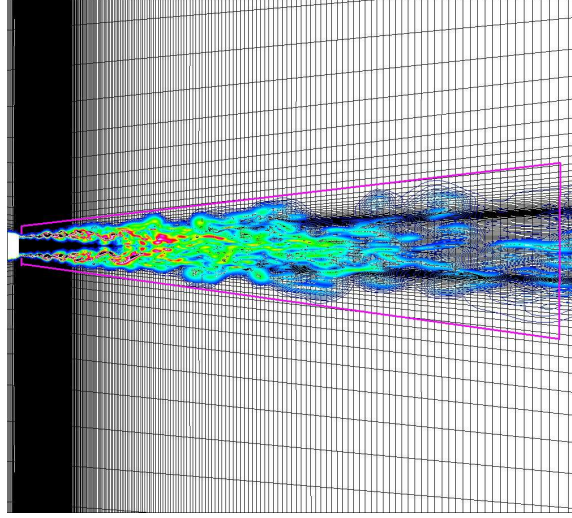

Figure 10. LES computation of Mach 0.9 cold jet: instantaneous vorticity field, computational grid, and FWH surface.
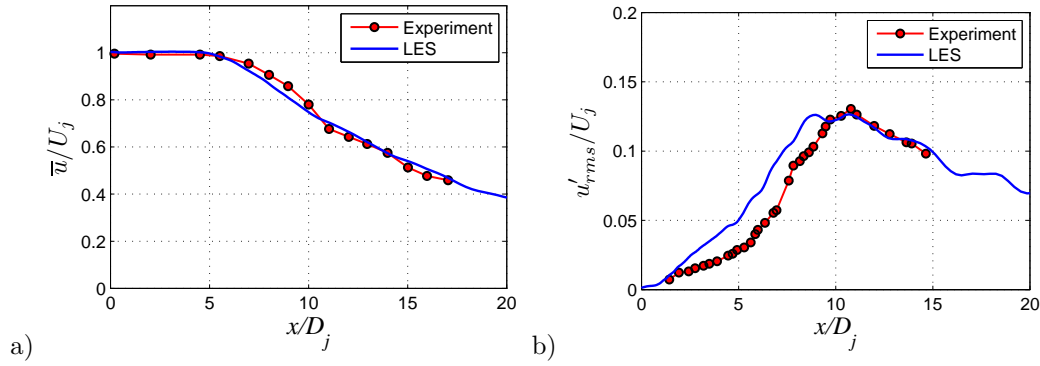

Figure 11. Centerline distributions in LES-computed Mach 0.9 jet, with comparison to the experiments of Lau *et al.*[25] a) Mean axial velocity; b) rms axial velocity.

Figure 10 depicts a snapshot of the instantaneous vorticity field, the computational grid used, and the geometry of the Ffowcs Williams - Hawkings (FWH) surface used for computing the radiated sound. Figure 11 plots the axial distributions of mean and rms axial velocity along the jet centerline. The agreement with the experiments of Lau *et al.*[25] is very good. The predictions of the far-field sound pressure levels are compared with experimental measurements in Fig. 12. The agreement is reasonable in the Strouhal number range [0.1, 2.0]. These results, while preliminary, indicate that the LES is producing physically meaningful data.

V.B. Space-Time Correlations

The LES solution allows calculation of the space-time correlation anywhere inside and outside the jet flow within the computational domain. Stationarity in time is assumed. We examine the axial space-time correlation of pressure, in the normalized form

$$R_{pp}(x, y; \xi_x, \tau) = \frac{< p'(x, y, t) \, p'(x + \xi_x, y, t + \tau) >}{p'_{rms}(x, y) p'_{rms}(x + \xi_x, y)} \tag{12}$$

where $<>$ denotes the time average. The correlation for u' produced practically identical results. Example space-time correlations are plotted in Fig. 13.

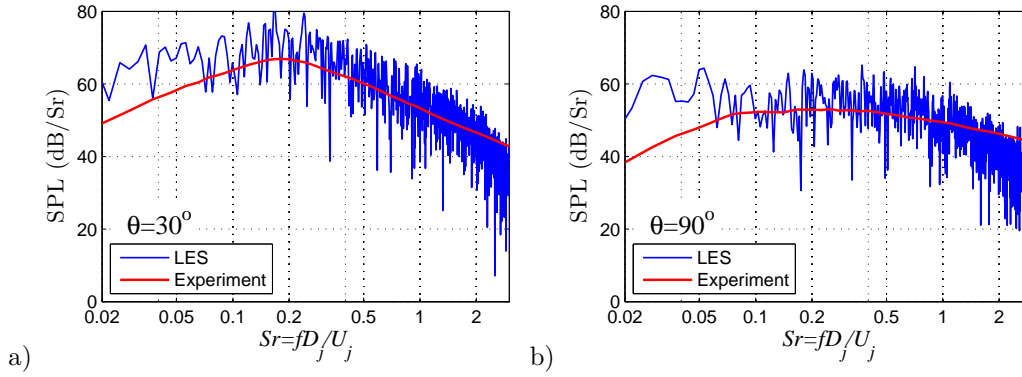American Institute of Aeronautics and Astronautics

Figure 12. Far-field sound pressure level spectra (r/D_j=100) of LES-computed Mach 0.9 jet, with comparisons to experimental measurements at UCI. a) $\theta = 30°$; b) $\theta = 90°$.
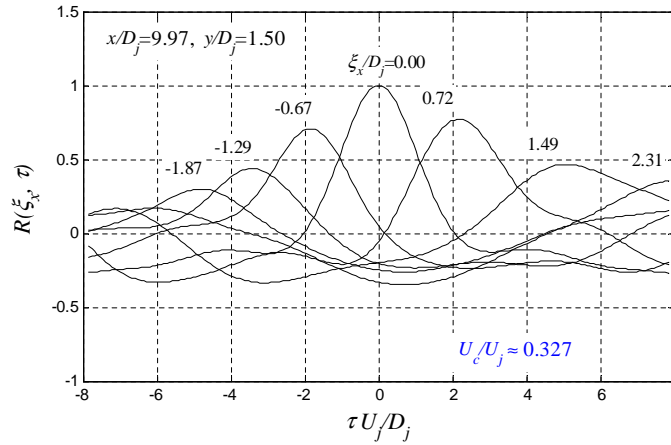

Figure 13. Space-time correlation of pressure at $x/D_j = 10, y/D_j = 1.0$.

Computation of the convective velocity at point (x_{i_0}, y_{j_0}) of the computational grid involved the space-time correlations at very small axial separations around this point, $\xi_{x,i} = x_i - x_{i_0}$, $i = -2, -1, 1, 2$, where x_i is the computational axial vector. Small separations were used because the statistics in space are not stationary. Because each correlation function comprises a discrete set of points, to accurately locate the maximum value of the correlation a seventh-order polynomial was fitted around the peak of the correlation curve. The time separation corresponding to the maximum value of the polynomial (i.e., the root of the derivative), τ_i, was then calculated using a Newton-Raphson iteration method. The convective velocity was obtained from

$$U_c(x_{i_0}, y_{j_0}) = \frac{1}{4} \sum_{i=-2,-1,1,2} \frac{\xi_{x,i}}{\tau_i} \qquad (13)$$

Figure 14 shows contour maps of U_c/U_j on the $x - y$ plane, along with the distributions of mean axial velocity and turbulent kinetic energy. Because this is a subsonic jet, the convective velocity inside the jet flow is subsonic. Note that computation of U_c in the potential core near the nozzle exit was not reliable because the pressure fluctuations there are very weak. For a given axial location, U_c declines with radial location from the centerline until it reaches a minimum value inside the jet near the edge of the jet. This is consistent with past experimental works that found that U_c "follows" the mean velocity $\overline{u}$ inside the jet. With further increase in radial location, U_c rises and transitions from subsonic to supersonic. The transition point here is $U_c/U_j = 1.2$ and, as shown in Fig. 14c, it defines a conical-like surface around the jet. Defining the edge of the jet as the boundary between rotational and irrotational flow (a quantitative criterion will follow), the pressure field on the edge contains the full hydrodynamic component which can be thought of as the footprint of the turbulent motion inside the jet. The pressure field on the edge also contains an acoustic (propagating) component, which in this case is weak because the jet is subsonic. Because this is not a very

American Institute of Aeronautics and Astronautics

high speed jet, it is reasonable to treat the acoustic field on the edge and outward as linear, and thus apply linear propagation methods. The hydrodynamic field is evanescent and thus decays rapidly with distance, the decay rate being proportional to the local characteristic frequency[26] (or inversely proportional the local coherence scale). At some radial distance, only the acoustic component remains. This is the transition point where U_c become sonic. Outside the transition "cone", the entire pressure field is acoustic.
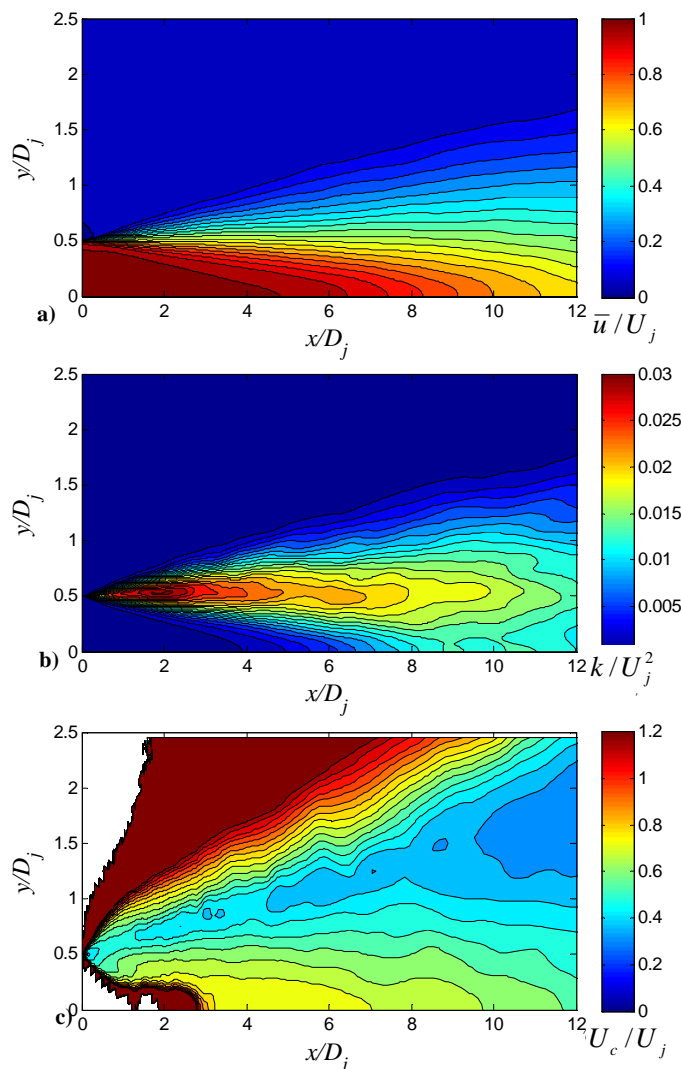

Figure 14. Contour maps on $x-y$ plane of statistics for LES-computed jet: a) mean axial velocity $\overline{u}/U_j$; b) turbulent kinetic energy k/U_j^2; and c) convective velocity U_c/U_j.

V.C.   Conditions at the Edge of the Jet

Any surface surrounding the jet that does not include the vortical field can be used as a "source surface" to propagate outward and compute the far field sound. That surface would have a particular distribution of U_c, depending on its shape (e.g., cone, cylinder, etc), and its distance from the jet axis. However, as pointed out earlier, there is only one such surface that contains the full hydrodynamic component of the pressure field, i.e., the signature of the turbulent motion of the eddies inside the jet. This surface is the edge of the jet, defined now more precisely as the closest surface to the jet centerline on and outside of which the propagation of pressure perturbation is governed by the homogeneous linear wave equation. If a connection is to be made between a fluid-mechanical velocity and a convective velocity in the linear pressure field, the latter would need to be defined on the edge surface. Outside the edge surface, the hydrodynamic information is lost quickly. Accordingly, we compare U_c/U_j on the edge to U_c/U_j at the location of the peak turbulent

American Institute of Aeronautics and Astronautics

kinetic energy. The edge $y_{edge}(x)$ is now defined as the radial position where the radial gradient of the mean axial velocity, normalized bv its local peak value, is less than a given threshold:

$$\frac{|d\overline{u}/dy|(x, y_{edge}(x))}{|d\overline{u}/dy|_{max}(x)} \leq \kappa \tag{14}$$

A justification for this criterion is provided in Appendix A. Experimentation with various thresholds $\kappa = 0.05, 0.02, 0.01$ gave similar results for y_{edge} because the radial velocity gradient decays very rapidly with radial distance at the edge of the jet. Here we choose $\kappa = 0.05$. Figure 15 illustrates the determination of U_c and clarifies the concepts discussed above. Plotted are the radial distributions of velocity gradient magnitude (normalized by the maximum value), $\overline{u}/U_j$, and U_c/U_j at $x/D_j = 4.0$. The figure allows a more quantitative assessment of the trends discussed in connection with contour maps of Fig. 14. Starting from the jet centerline, U_c initially follows the mean velocity, reaches a minimum, and then starts rising *within* the rotational region of the jet. The edge of the jet, y_{edge}, is defined as the point where $|d\overline{u}/dy|/|d\overline{u}/dy|_{max}=0.05$. The corresponding $U_c/U_j = 0.57$, which is our selection for the convective speed at this particular $x-$location. For $y > y_{edge}$, U_c/U_j keeps increasing and the pressure field becomes purely acoustic at $U_c/U_j = 1.2$, which corresponds to $U_c/a_\infty = 1.0$.

Figure 16 plots the axial distribution of convective velocity as determined from the space-time correlation at $y = y_{edge}(x)$ and from the mean velocity at the locus of peak turbulent kinetic energy. The two results match quite well within the potential core length of the jet. With x/D_j increasing beyond ~ 6, there is a departure of the two curves. Noting that the principal noise sources for this jet are contained within the first ten or so diameters, the overall agreement is deemed reasonable. Further work is needed to refine the U_c selection criterion for the jet region downstream of the potential core.
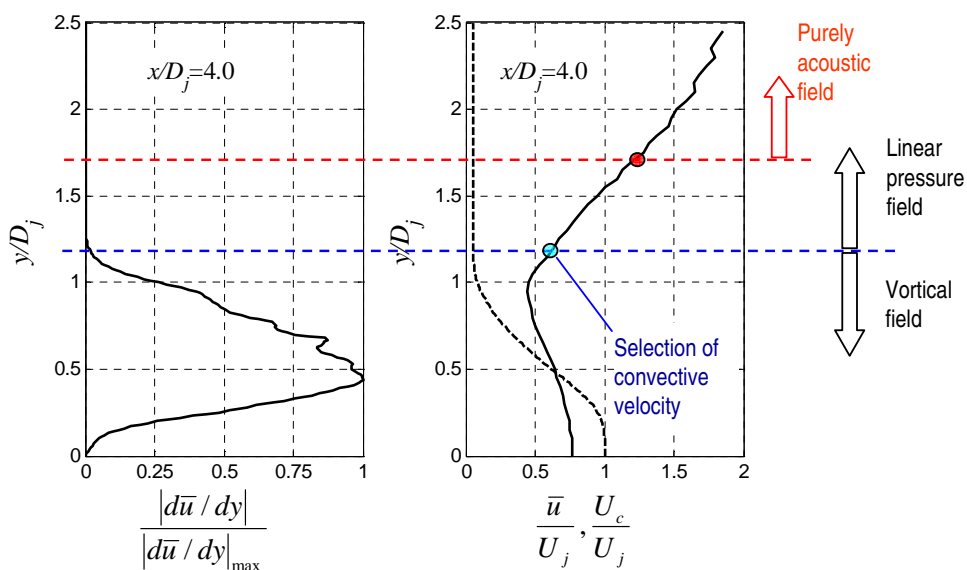

Figure 15. Radial distributions of mean velocity gradient, normalized by maximum value, and convective velocity. Dashed line on right subfigure plots the mean axial velocity. Relevant jet regions are identified.

VI. Conclusions

The Lighthill acoustic analogy indicates that substantial noise reduction is possible in high-speed jets by reducing the radiation efficiency. This entails reducing the convective Mach number of the eddies whose footprint is sensed in the near pressure field. In dual-stream jets, local reduction in convective Mach number is possible by inducing asymmetry in the plume that redistributes the most energetic eddies from the fast inner stream to the slower outer stream on the underside of the jet. This results in substantial noise reduction in the direction of peak emission.

Despite a significant reduction of the turbulent kinetic energy on the underside of the asymmetric jet, RANS-based acoustic analogy fails to predict the noise reduction unless a physical model for the convective velocity is implemented. This is accomplished here by defining the convective velocity as the mean

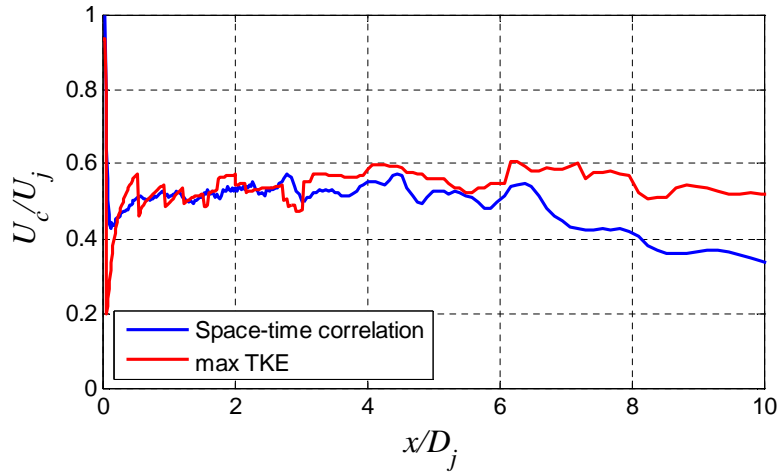American Institute of Aeronautics and Astronautics

Figure 16. Normalized convective velocity determined from space-time correlations at the edge of the jet and from the mean axial velocity at the location of peak turbulent kinetic energy.

velocity at the location of the peak turbulent kinetic energy. The resulting distribution of convective Mach number appears the capture the physical evolution of turbulent eddies in the dual-stream axisymmetric and asymmetric jets. Consequently, the RANS-based acoustic analogy predicts with reasonable fidelity the noise reduction measured experimentally. Importantly, it is shown that the reduction in the source strength is caused primarily by the reduction in radiation efficiency.

A large eddy simulation of a single-stream high-subsonic jet allows determination of the convective velocity through space-time correlations throughout the computational domain. The convective velocity at the edge of the jet, defined as the boundary between the inner rotational field and the outer linear pressure field, is close to the mean axial velocity at the location of peak kinetic energy within the potential core region of the jet. This suggests the validity of the aforementioned model for the convective velocity and thus provides a tool for RANS-based acoustic analogy models to accurately capture the radiation efficiency and its reduction.

Acknowledgments

Appendix A: Definition of Linear Pressure Field Boundary

We discuss the selection of a criterion to define the boundary between the jet flow and the linear pressure field generated by the jet. We define the linear pressure field as the region surrounding the jet where the propagation of pressure is governed by the homogeneous linear wave equation. To quantify this definition, we examine an axisymmetric flow on the (x, y) plane with unidirectional mean velocity $\overline{\mathbf{u}} = (\overline{u}(y), 0, 0)$ and mean speed of sound $\overline{a}(y)$. We impose small (linear) perturbations $\mathbf{u}' = (u', v')$, ρ', and p'. The perturbations are thus governed by the linear Euler equations, which under the aforementioned conditions yield the following equation for the pressure:[27]

$$\frac{\overline{D}}{Dt}\left[\frac{1}{\overline{a}^2}\frac{\overline{D}^2 p'}{Dt^2} - \nabla^2 p'\right] = -2\frac{d\overline{u}}{dy}\frac{\partial^2 p'}{\partial x \partial y}$$

where $\overline{D}/Dt \equiv \partial/\partial t + \overline{u}\partial/\partial x$. When the right hand vanishes, the pressure is governed by the homogeneous convective wave equation and thus our criterion is satisfied. Order of magnitude analysis yields

$$\frac{a}{\lambda^3}[p'] = \frac{d\overline{u}}{dy}\frac{1}{\lambda^2}[p']$$

where λ is the acoustic wavelength. Letting $f_c = a/\lambda$ denote the characteristic frequency of noise emission, the above is rewritten as

$$[p'] \ = \frac{1}{f_c} \frac{d\overline{u}}{dy} [p']$$

Hence the criterion for the linear pressure field is

$$\frac{1}{f_c} \frac{d\overline{u}}{dy} \to 0$$

Extending this relation to a slowly developing jet flow, the characteristic frequency is connected to the integral thickness $\delta(x)$ and the mean centerline jet velocity $u_0(x)$ via

$$f_c \ = \ \frac{u_0(x)}{\delta(x)}$$

Selecting δ as the vorticity thickness,

$$\delta = \frac{u_0}{(d\overline{u}/dy)_{max}}$$

the characteristic frequency is

$$f_c \ = (d\overline{u}/dy)_{max}$$

and thus the criterion becomes

$$\frac{d\overline{u}/dy}{(d\overline{u}/dy)_{max}} \to 0$$

References

[1] Aubert, A. and McKinley, R., "Measurements of Jet Noise Aboard US Navy Aircraft Carriers," AIAA 2011-6947, Sept. 2011.

[2] Morris, P. and McLaughlin, D., "High Speed Jet Noise Reduction - Past Progress and Future Possibilities," AIAA 2013-0006, Jan. 2013.

[3] Papamoschou, D., "Mach Wave Elimination in Supersonic Jets," *AIAA Journal*, Vol. 35, No. 10, 1997, pp. 1604–1611.

[4] Papamoschou, D. and Debiasi, M., "Directional Suppression of Noise from a High-Speed Jet," *AIAA Journal*, Vol. 39, No. 3, 2001, pp. 380–387.

[5] Zaman, K., "Noise- and Flow-Field of Jets From an Eccentric Coannular Nozzle," AIAA 2004-0005, January 2004.

[6] Papamoschou, D., "Fan Flow Deflection in Simulated Turbofan Exhaust," *AIAA Journal*, Vol. 44, No. 12, 2006, pp. 3088–3097.

[7] Brown, C., Bridges, J., and Henderson, B., "Offset-Stream Technology Test - Summary of Results," AIAA 2007-3664, January 2007.

[8] Papamoschou, D., Johnson, A., and Phong, V., "Aeroacoustics of Three-Stream High-Speed Jets from Coaxial and Asymmetric Nozzles," AIAA 2013-0007, Jan. 2013.

[9] Papamoschou, D. and Rostamimonjezi, S., "Modeling of Noise Reduction for Turbulent Jets with Induced Asymmetry," AIAA 2012-2158, June 2012.

[10] Morris, P. J. and Farassat, F., "Acoustic Analogy and Alternative Theories for Jet Noise Prediction," *AIAA Journal*, Vol. 40, No. 4, 2002, pp. 671–680.

[11] Viswanathan, K., Underbrink, J., and Brusniak, L., "Space-Time Correlation Measurements in the Near Field of Jets," *AIAA Journal*, Vol. 49, 2011, pp. 1577–1599.

[12] Xiong, J., Nielsen, P., Liu, F., and Papamoschou, D., "Computation of High-Speed Coaxial Jets with Fan Flow Deflection," *AIAA Journal*, Vol. 48, No. 10, 2010, pp. 2249–2262.

[13] Jameson, A., Schmidt, W., and Turkel, E., "Numerical Solutions of the Euler Equations by Finite Volume Methods Using Runge-Kutta Time Stepping Schemes," AIAA 1981-1259, January 1981.

[14] Menter, F., "Two-Equation Eddy-Viscosity Turbulence Models for Engineering Applications," *AIAA Journal*, Vol. 32, No. 8, 1994, pp. 1598–1605.

[15] Roe, P. L., "Approximate Riemann Solvers, Parameter Vectors and Difference Schemes," *Journal of Computational Physics*, Vol. 46, No. 2, 1980, pp. 357–378.

[16] Shur, M. L., Spalart, P. R., and Strelets, M. K., "Noise Prediction for Increasingly Complex Jets. Part I: Methods and Tests," *International Journal of Aeroacoustics*, Vol. 4, No. 3, 2005, pp. 213–246.

[17] Spalart, P. R., Jou, W. H., Strelets, M., and Allmaras, S. R., "Comments on the Feasibility of LES for Wings, and on a Hybrid RANS/LES Approach," 1st AFOSR Int. Conf. on DNS/LES, Ruston, LA, August 1997.

[18] Vold, H., Shah, P., Morris, P., Dongle, Y., and Papamoschou, D., "Axisymmetry and Azimuthal Modes in Jet Noise," AIAA 2012-2214, June 2012.

[19] Spalart, P. R. and Allmaras, S. R., "A One-Equation Turbulence Model for Aerodynamic Flows," AIAA 1992-0439, January 1992.

American Institute of Aeronautics and Astronautics

[20]Morris, P. and Zaman, K., "Velocity Measurements in Jets with Application to Jet Noise," *Journal of Sound and Vibration*, Vol. 329, 2010, pp. 394–414.

[21]Brown, G. and Roshko, A., "On Density Effects and Large Structure in Turbulent Mixing Layers," *Journal of Fluid Mechanics*, Vol. 64, 1974, pp. 775–816.

[22]Murakami, E. and Papamoschou, D., "Eddy Convection in Supersonic Coaxial Jets," *AIAA Journal*, Vol. 38, No. 4, 2000, pp. 628–635.

[23]Thurow, B., Naibo, J., Kim, J.-H., Lempert, W., and Samimy, M., "Issues with Measurements of the Convective Velocity of Large-Scale Structures in the Compressible Shear Layer of a Free Jet," *Physics of Fluids*, Vol. 20, 2008, pp. 066101–1–15.

[24]Karabasov, S., Afsar, M., Hynes, T., Dowling, A., McMullan, W., Pokora, C., Page, G., and Guirk, J., "Jet Noise: Acoustic Analogy Informed by Large Eddy Simulation," *AIAA Journal*, Vol. 48, No. 7, 2010, pp. 1312–1325.

[25]Lau, J., Morris, P., and Fisher, M., "Measurements in Subsonic and Supersonic Free Jets Using a Laser Velocimeter," *Journal of Fluid Mechanics*, Vol. 93, No. 1, 1979, pp. 1–27.

[26]Guitton, A., Jordan, P., and Laurendau, E., "Velocity Dependence of the Near Pressure Field of Subsonic Jets: Understanding the Associated Source Mechanisms," AIAA 2007-3661, June 2007.

[27]Bogey, C., Bailly, C., and Juve, D., "Computation of Flow Noise Using Source Terms in Linearized Euler's Equations," *AIAA Journal*, Vol. 40, No. 2, 2002, pp. 235–243.

American Institute of Aeronautics and Astronautics